Slovak University of Technology in Bratislava, Faculty of Civil Engineering,

Department of Concrete Structures and Bridges

Michaela Štefanovičová

Dissertation Thesis Abstract

The Effect of Bond of GFRP Reinforcement on Bending Behaviour of GFRP-reinforced Concrete Members

to obtain the Academic Title of „philosophiae doctor“ abbreviated as „PhD.“

in the doctorate degree study programme:
Theory and Structures of Civil Engineering Works

in the field of study:
Civil Engineering

Form of Study:
full-time

Place and Date:
Bratislava, 03.05.2024

Dissertation Thesis has been prepared at
Faculty of Civil Engineering, Department of Concrete Structures and Bridges

Submitter: Ing. Michaela Štefanovičová
Department of Concrete Structures and Bridges
Faculty of Civil Engineering
Slovak University of Technology in Bratislava
Radlinského 11, 810 05 Bratislava

Supervisor: doc. Ing. Róbert Sonnenschein, PhD.
Department of Concrete Structures and Bridges
Faculty of Civil Engineering
Slovak University of Technology in Bratislava
Radlinského 11, 810 05 Bratislava

Consultant: doc. Ing. Katarína Gajdošová, PhD.
Department of Concrete Structures and Bridges
Faculty of Civil Engineering
Slovak University of Technology in Bratislava
Radlinského 11, 810 05 Bratislava

Dissertation Thesis Abstract was sent: 2024
(Date of sending)

Dissertation Thesis Defence will be held on 2024
at.....(am/pm) at Department of Concrete Structures and Bridges, Faculty of Civil Engineering, STU in Bratislava , Radlinského 11, 810 05 Bratislava.

.....
Prof. Ing. Stanislav Unčík, PhD.
Dean of Faculty of Civil Engineering STU,

Acknowledgments

I extend heartfelt gratitude to Assoc. Prof. Ing. Róbert Sonnenschein, PhD, and Prof. Ing. Katarína Gajdošová, PhD, for their invaluable guidance and mentorship. Special thanks to Dr. Ali Hadigheh for enabling my stay at the University of Sydney. I am also thankful to the Slovak Academic Information Agency for financial support.

My deepest appreciation goes to my family, partner, friends, and colleagues for their unwavering encouragement and support. I am also grateful to the manufacturers of GFRP reinforcement for providing materials.

This dissertation represents a significant academic achievement and personal growth. The journey has deepened my understanding of GFRP bars in reinforced concrete and contributed to my development as a scholar.

I am deeply grateful to everyone who has been part of this endeavor.

Abstract

This dissertation thesis investigates the impact of GFRP bar bond strength on the bending behaviour of GFRP-reinforced concrete members. Extensive research has highlighted the critical role of surface treatment in the bond development of GFRP reinforcement with concrete, significantly influencing crack formation in GFRP-reinforced elements. The first part of the experimental program validates the bond strength of locally available GFRP reinforcements with two different surface treatments using pull-out and bond beam tests. Subsequently, the second part examines the flexural behaviour of simple and continuous beams reinforced with GFRP bars. The study aims to explore the effects of GFRP bar bond strength on the crack formation and bending resistance, as well as investigate the potential redistribution of moments in continuous beams with varying reinforcement ratios at the intermediate support section of GFRP-reinforced beams. Ultimately, the research seeks to assess the feasibility of employing GFRP reinforcement in statically indeterminate elements.

Table of Contents

1. Introduction

The use of Fibre-reinforced polymer (FRP) bars as an alternative to steel reinforcements in concrete structures has surged in recent decades due to steel's susceptibility to corrosion, leading to the degradation of concrete. Consequently, there's been a notable demand for non-corrosive, chemically resistant, and magnetically neutral FRP reinforcements. Among FRP bars, Glass Fiber-Reinforced Polymer (GFRP) bars are frequently chosen due to their accessibility and cost-efficiency despite their lower modulus of elasticity compared to steel bars, resulting in higher deformations of GFRP-reinforced concrete (GFRP RC) members.

Unique design considerations and adherence to specific guidelines are necessary for GFRP RC structures due to the distinct bond behaviour of FRP reinforcement with concrete compared to steel reinforcement. Extensive research has been dedicated to investigating FRP reinforcement bond behaviour, considering varied mechanical properties and surface configurations among manufacturers. The nonductile behaviour of FRP reinforcement influences the design approach for FRP RC members subjected to bending, impacting load-bearing capacity and moment redistribution ability.

Experimental results from continuous beams reinforced with GFRP indicate potential debonding issues over intermediate support sections, affecting structural integrity. The impact of bond properties is crucial not only for meeting ultimate limit states but also for ensuring compliance with serviceability criteria, particularly concerning crack control. This underscores the significance of the bond-dependent coefficient (k_b) in predicting crack width and overall structural performance.

2. The current state of knowledge

The current state of knowledge of GFRP bars' mechanical properties is outlined, highlighting their differences from traditional steel reinforcements. The bond mechanism between GFRP bars and concrete is explained, covering key parameters influencing this bond. Additionally, an overview of current code approaches for determining GFRP bar bond strength is provided alongside experimental methods aligned with standards. Furthermore, current code approaches for designing FRP RC members subjected to bending are summarised, and major concerns regarding the design of continuous GFRP-reinforced structures are introduced.

Variability in GFRP bars' mechanical properties and surface configurations, often stemming from manufacturer differences, is discussed. Recent research underscores surface treatment as a critical parameter affecting bond quality. The bond between GFRP bars and concrete further influences crack formation in GFRP RC members, emphasizing the importance of serviceability limit state criteria (cracking and deflection) in their design. Lastly, the linear elastic stress-strain relationship of FRP bars raises concerns about their ability to redistribute moments in continuous members. The member's capacity for moment redistribution is typically contingent on its ability to undergo plastic deformation, a property associated with sufficient ductility.

3. Objectives of the dissertation thesis

This dissertation thesis aims to investigate the bond behaviour of GFRP bars to concrete and the influence of the bond on the bending behaviour of continuous beams. Therefore, the following objectives are presented in this thesis:

- Compare experimentally verified bond behaviour of locally available GFRP bars featuring various surface treatments using two different testing methods: beam test according to RILEM [1] and pull-out test according to ACI 440.3R-12 [2].
- Based on experimental findings, analysis of the effect of the test method and surface treatment on the bond between GFRP bars and concrete, as well as identifying differences in bond behaviour between the tested GFRP bars and traditional steel bars.
- Compare experimentally verified bending behaviour of continuous and simple GFRP RC beams involving various reinforcement ratios at the intermediate support section and GFRP bars with different surface treatments.
- Based on experimental results, analysis of the effect of the reinforcement ratio at the intermediate support on load-bearing capacity, moment redistribution, crack widths and deflections of continuous GFRP RC beams.
- Based on experimental results, examination of the effect of bond properties of GFRP bars on bending capacity, crack propagation and crack widths of continuous and simple GFRP RC beams.
- Based on experimental results and current codes of practice, the determination of bond-dependent coefficient k_b value of locally available GFRP bars.

4. Experimental program

The experimental program is structured into three distinct segments. The initial part provides an overview of the material properties of the reinforcement and concrete utilized in all test specimens. The subsequent section focuses on the experimental assessment of the bond between the reinforcement and concrete. Lastly, the third part examines the bending behaviour of both simple and continuous beams.

4.1. Material properties

The material properties of reinforcement and concrete used in tested specimens are described in this chapter. All tested specimens were prepared in the Central Laboratory of the Slovak University of Technology in Bratislava. All the specimens and material samples were kept under the same curing conditions to minimize the environmental influence.

4.1.1. Reinforcement

Three different types of reinforcement were used in the samples: steel reinforcement B500B, GFRP reinforcement with the sand-coated surface (SC), and GFRP reinforcement with the helically wrapped surface (HW).

The sand-coated GFRP bars (Figure 4.1) are from a company located in the Czech Republic (PREFA KOMPOZITY, a.s.). These GFRP bars are produced by pultrusion from continuous longitudinal fibres impregnated with vinyl-ester resin: the core of the bar comprises 75-80% (per weight) of E-CR glass fibres and 20-25% (per weight) of vinyl-ester resin [3] The surface treatment is composed of silica sand with grain thickness ranging from 0.26 to 0.74 mm to enhance the bond properties of the bars.

Figure 4.1 GFRP reinforcement with SC surface.

The GFRP bars with the helically wrapped surface (HW) (Figure 4.2) are from a company in the Slovak Republic (Tesla FiberoX s. r. o.). They are also produced by pultrusion from continuous longitudinal fibres impregnated with epoxy resin: the content of E-CR glass is 72-77% (per weight) and 23-28% (per weight) of epoxy resin [4] The helical wrapping on the surface is comprised of the same materials as the bar's core.

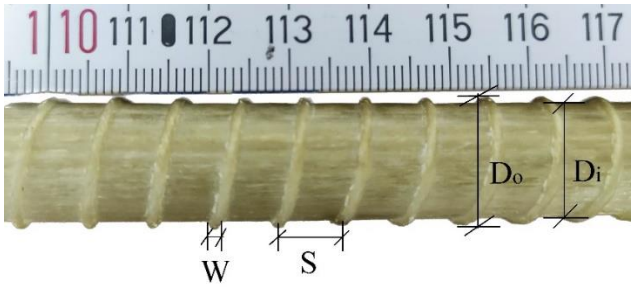

Figure 4.2 GFRP reinforcement with HW surface.

The obtained tensile properties in tensile tests of GFRP bars and the tensile properties provided by the manufacturer are summarised in Table 4.1. The stress-strain curves obtained in the tensile tests of GFRP bars are plotted in Figure 4.3.

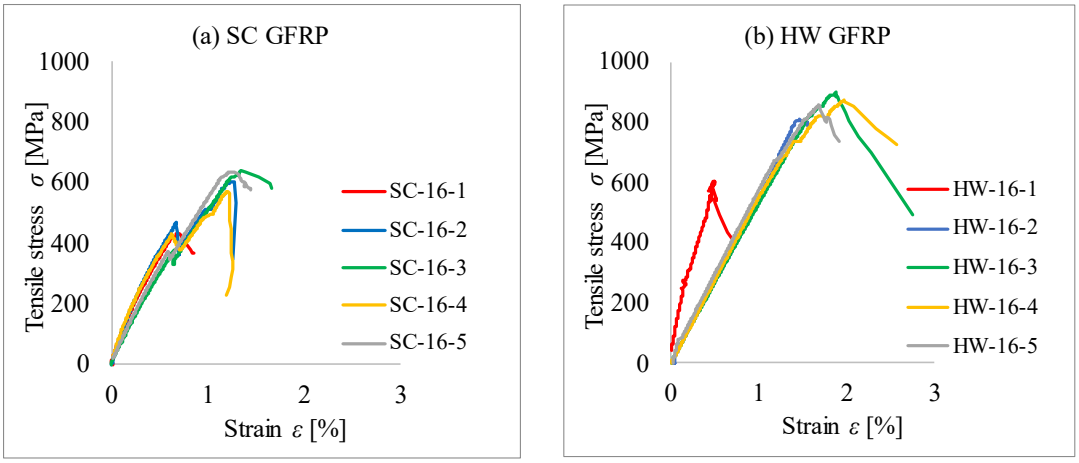

Figure 4.3 Tensile stress-strain curve of (a) SC GFRP bars; (b) HW GFRP bars

Table 4.1 Mechanical properties of GFRP bars

Type of the bar	Sample	F_u [kN]	$A_{f,bar}$ [mm^2]	f_{fu} [MPa]	ε_{fu} [%]	E_f [GPa]	f_m [MPa]	E_m [GPa]
Sand-coated GFRP	SC-16-1	86.5	186.5	464	0.58	79.9	>1100	>50
	SC-16-2	121.4	186.5	651	0.84	77.7		
	SC-16-3	119.5	186.5	641	1.15	55.6		
	SC-16-4	114.8	186.5	616	0.82	75.1		
	SC-16-5	128.2	186.5	687	1.15	59.8		
	Average	**114.1**	**186.5**	**649**	**0.99**	**67.1**		
Helically wrapped GFRP	HW-16-1	95.4	157.5	606	0.47	128.6	>1000	>55
	HW-16-2	127.7	157.5	811	1.53	53.1		
	HW-16-3	142.2	157.5	903	1.71	52.8		
	HW-16-4	137.7	157.5	874	1.58	55.4		
	HW-16-5	135.2	157.5	859	1.53	56.3		
	Average	**135.7**	**157.5**	**862**	**1.59**	**54.4**		

F_u is the ultimate load; $A_{f,bar}$ is the assumed area of one FRP bar; f_{fu} is the ultimate tensile strength of GFRP bar; ε_{fu} is the ultimate strain of GFRP in tension; E_f is the modulus of elasticity of GFRP bar; f_m is the tensile strength provided by the manufacturer; E_m is the modulus of elasticity provided by the manufacturer.
Note: The first samples from both GFRP bar types, SC-16-1 and HW-16-1, reached significantly lower tensile strength than the rest; therefore, they are not considered in the average values.

Compared to the values given by manufacturers, the reached tensile strength values (f_{fu}) are significantly lower, specifically by 41% on average in SC GFRP bars and 14% in HW GFRP bars. On the other hand, the reached modulus of elasticity (E_f) of SC GFRP is, on average, 34% higher than the value provided by the manufacturer. On the contrary, the average modulus of elasticity (E_f) of HW GFRP bars from the tensile test is in good agreement with the value provided by the manufacturer.

The tensile properties of reinforcing steel of class B500B were determined according to the standard ISO 6892-1 [5] Tested diameters were 8 mm for stirrups and 16 mm for longitudinal reinforcement. Tensile tests on six samples with a length of 1000 mm were performed from each diameter. The steel bars with diameter of 16 mm reached average yield strength (f_y) of 580 MPa at strain (ε_y) of 2.7‰ and had average modulus of electricity 214 GPa.

4.1.2. Concrete

All specimens of the same industrially manufactured concrete mixture were cast at once in the Central Laboratory of the Slovak University of Technology in Bratislava. The

strength properties of concrete were tested at the same time as the beam bending tests were performed. The mechanical properties of concrete are summarised in Table 4.2.

Table 4.2 Mechanical properties of concrete

Specimen	$f_{c.cube}$ **[MPa]**	$f_{c.cyl}$ **[MPa]**	E_c **[GPa]**	$f_{ct.sp}$* **[MPa]**
1	54.8	36.63	38	3.74
2	52.29	44.95	37	4.26
3	52.14	33.44	36.5	3.53
4	54.28	35.4	38.5	3.66
5	51.77	39.93	39	3.95
6	52.38	41.51	37	4.05
Avarage	**53**	**39**	**38**	**3.9**

$f_{c,cube}$ is the compressive cube strength of concrete, $f_{c,cyl}$ is the compressive cylinder strength of concrete, E_c is the modulus of elasticity of concrete, $f_{ct,sp}$* is the calculated tensile strength of splitting concrete

4.2. Experimental determination of bond

The bond behaviour of 3 types of reinforcement with a nominal diameter of 16 mm was investigated: steel reinforcement, sand-coated GFRP reinforcement, and helically wrapped GFRP reinforcement. The bond behaviour of GFRP bars is specimen-configuration dependent. Therefore, two different test methods were used to determine the bond strength. Overall, nine beam tests were performed following RILEM [1] and nine pull-out tests according to ACI 440.3R-12 [2] For each type of reinforcement and test method, three specimens were tested.

4.2.1. Beam bond test

The geometry of the beam specimen and test set-up of the beam bond test are displayed in Figures 4.4 and 4.5. The test setup was composed of a universal, open-structure flexural frame with a capacity of 300 kN and measuring devices. The load was applied at two points at the speed of 50 N/s in 2 kN steps or 100 N/s in 5 kN steps and measured with the electronic load cell of the testing machine. Two linear variable differential transformers (LVDTs) with a precision of 0.01 mm were used to measure the slip of the bar, i.e., one at the loaded end in the centre of the specimen and one at the free end of the bar tested. The strain in the bar at the midspan cross-section was measured with a strain gauge.

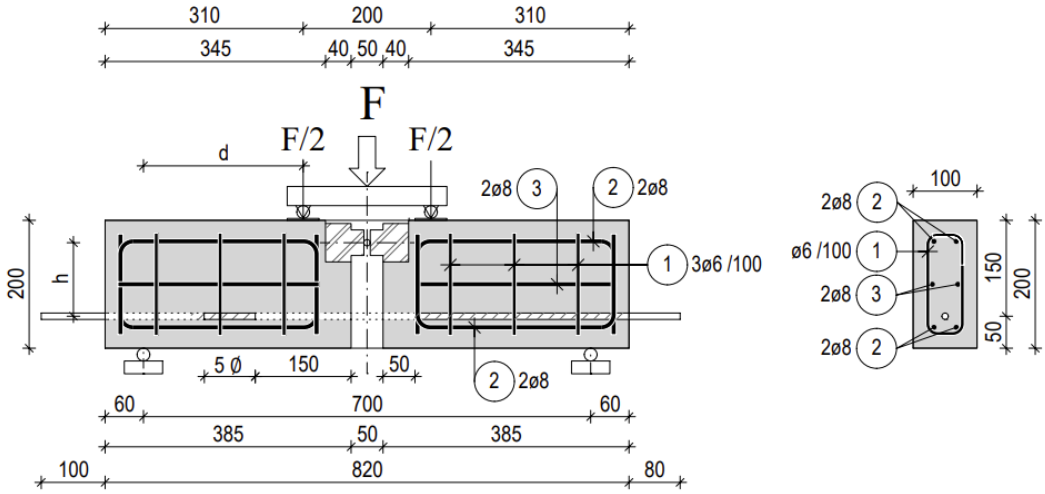

Figure 4.4 Geometry of the beam specimen (dimensions in mm)

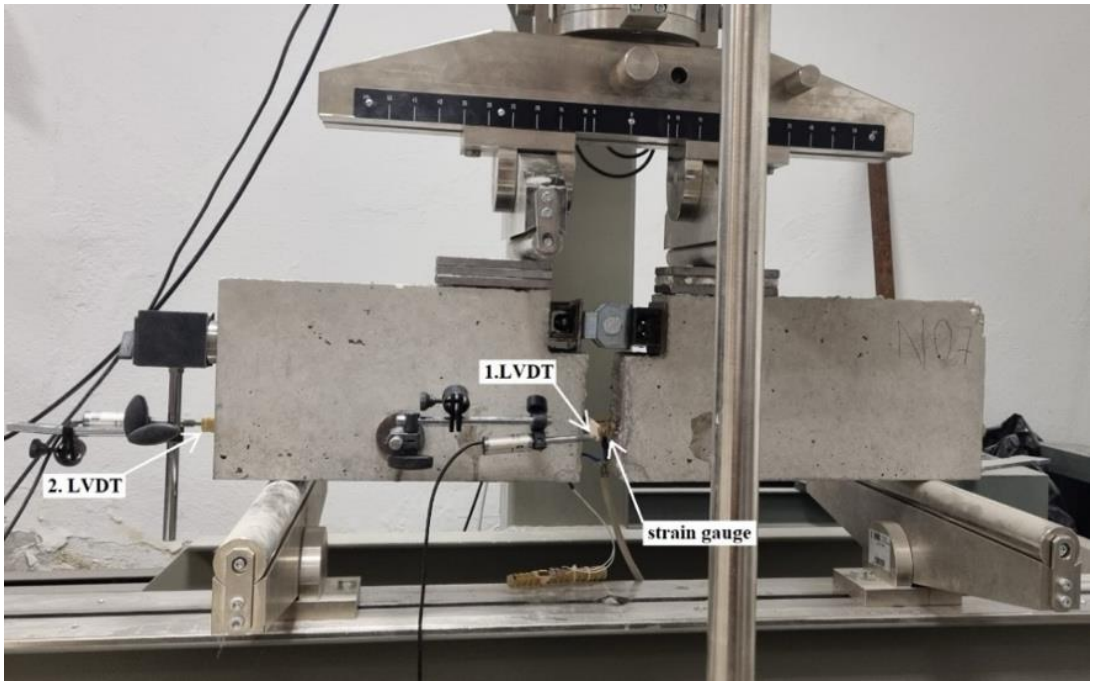

Figure 4.5 Beam bond test setup

4.2.2. Pull-out test

The specimen for the pull-out test consists of a cube with dimensions of 200 x 200 x 200 mm and a centrally placed single GFRP or steel reinforcement, see Figure 4.6 (c). A combined tension/compression testing machine with a capacity of 500 kN was used for the pull-out test. The load was applied at a 10 mm/min rate by pulling the loaded end of the specimen. The slip at the free end of the bar was measured with a linear variable differential transformer (LVDT). The strain at the loaded end of the bar was measured with a strain gauge. Figure 4.12 (a, b) displays the pull-out test setup.

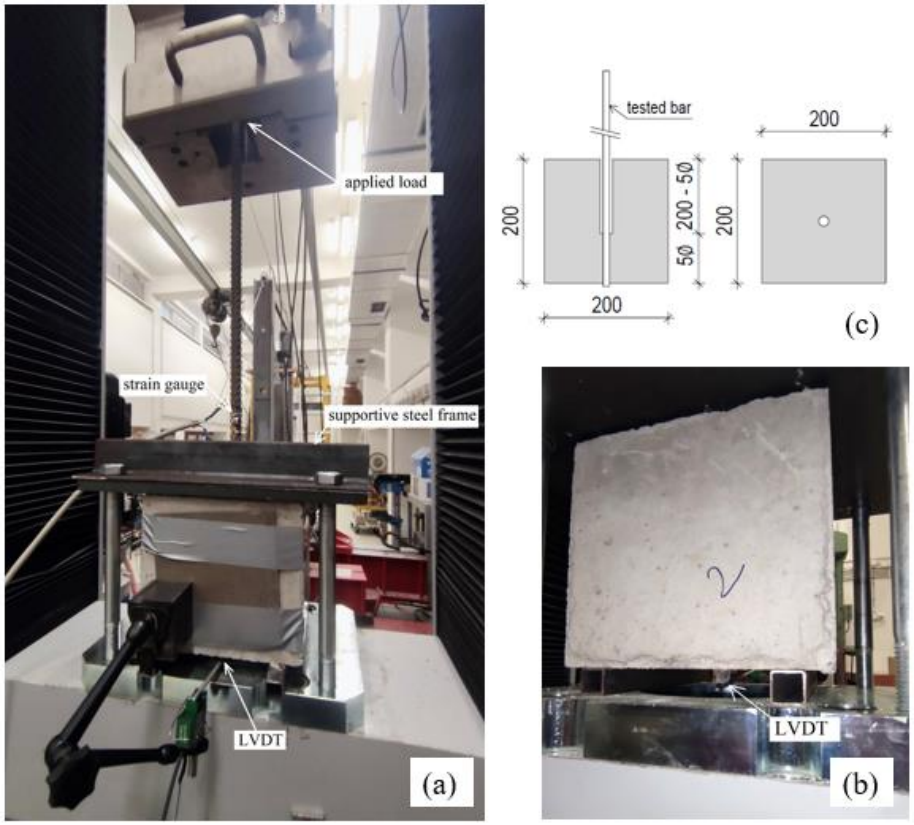

Figure 4.6 (a) Pull-out test setup, (b) LVDT at the free end of the bar, (c) Geometry of the specimen for the pull-out test (dimensions in mm)

4.2.3. Test results and discussion

The comparison of bond strength values ($\tau_{b.max}$) from both testing methods in Figure 4.7 (a) shows the following. The bond strength values ($\tau_{b.max}$) of steel bars obtained from both test methods are consistent; the average pull-out and beam bond test values vary only by 1%. Overall, the values differ only within 2 MPa. On the other hand, in the case of GFRP bars, the beam bond test provides higher bond strength values ($\tau_{b.max}$) than the pull-out test, on average by 3% for the SC GFRP bars and 23% for HW GFRP bars. This phenomenon was also observed in state-of-the-art studies where both test methods were used [6], [7], [8] The higher bond strength values ($\tau_{b.max}$) in the beam tests might come from the tension-stiffening of the concrete surrounding the reinforcing bar, which also contributes to transmitting and resisting the tensile force.

Generally, the results show higher bond strength ($\tau_{b.max}$) for steel bars than for GFRP bars. For example, in beam tests, the SC GFRP bars reached 78%, and HW GFRP bars only 36% of the steel bars' average bond strength ($\tau_{b.max}$). In pull-out tests, the ratio is 76% and 27% of the steel bars' average bond strength ($\tau_{b.max}$) by SC GFRP and HW GFRP bars, respectively. The percentage of the average bond strength of GFRP to steel bars is displayed in Figure 4.7 (b). The average bond strength ($\tau_{b.max}$) of SC GFRP bars is contrary to the HW GFRP bars, higher by 54% in the beam test and by 64% in the pull-out test, indicating that sand-coating of the GFRP bars' surface can significantly enhance the bond to concrete.

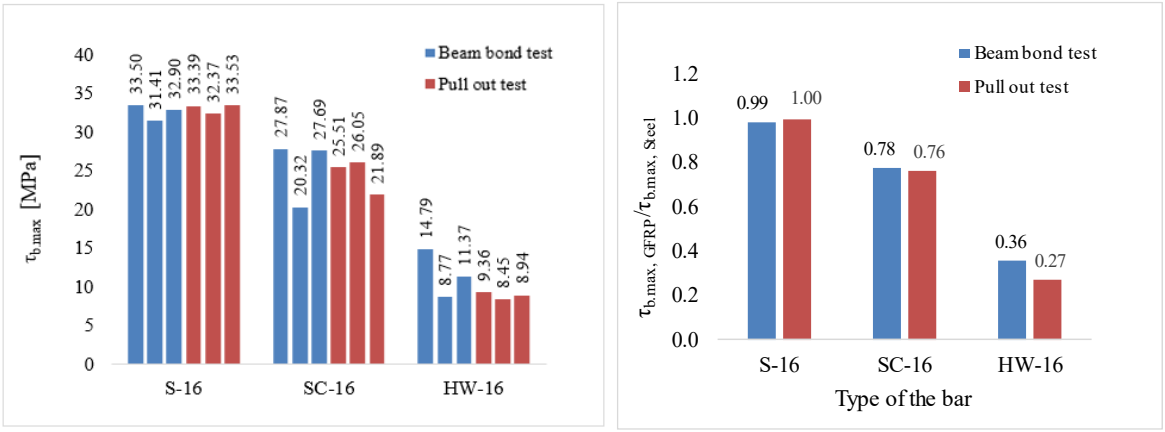

(a) (b)

Figure 4.7 (a) Bond strength of GFRP bars and steel bars, (b) Comparison of average bond strengths of GFRP bars and steel bars

4.2.3.1 Bond stress-slip relationship

The bond stress-slip diagrams obtained from beam and pull-out tests are plotted in Figures 4.8 and 4.9. The average curves of each reinforcement type are in red.

Generally, the initial stage of the bond stress–slip curve demonstrates a rapid increase in initial bond stress with minimal slip, representing the chemical adhesion strength ($\tau_{b.adh}$). After the chemical adhesion breaks down, the curve gradually ascends towards its peak point, representing the maximum bond strength ($\tau_{b.max}$). The gradual increase in the slip and bond stress is attributed to the mechanical interlock of the surface deformations. Once the bond strength reaches its peak ($\tau_{b.max}$), bond stress declines with increasing slip. At this point, friction mechanisms inhibit the formation of cylindrical cracks. The branch drops until bond stress remains nearly constant with high slip values, representing residual friction ($\tau_{b.res}$) [9] The described bond parameters of tested bars are displayed on average bond stress-strain curves obtained from pull-out tests in Figure 4.10. The beam bond test results are not used for this analysis because the frictional resistance can not be measured in beam bond tests.

The consistency in bond stress development between both testing methods reaffirms the reliability of the employed approaches. However, a significant variation is evident in the bond stress-slip diagram of HW GFRP bars. These bars exhibited heightened sensitivity to loading differences in the bond tests. In beam tests, loading ceases upon the failure of the first winding ring. In contrast, the pull-out test involves continued loading, enabling the observation of residual friction and a subsequent increase in the mechanical interlock of the bar.

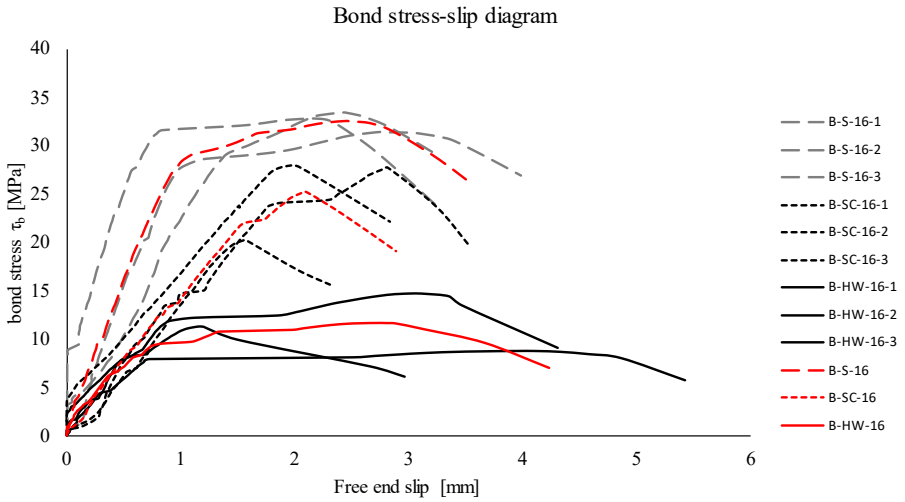

Figure 4.8 Bond stress–slip diagram of the beam test at the free end of the bar

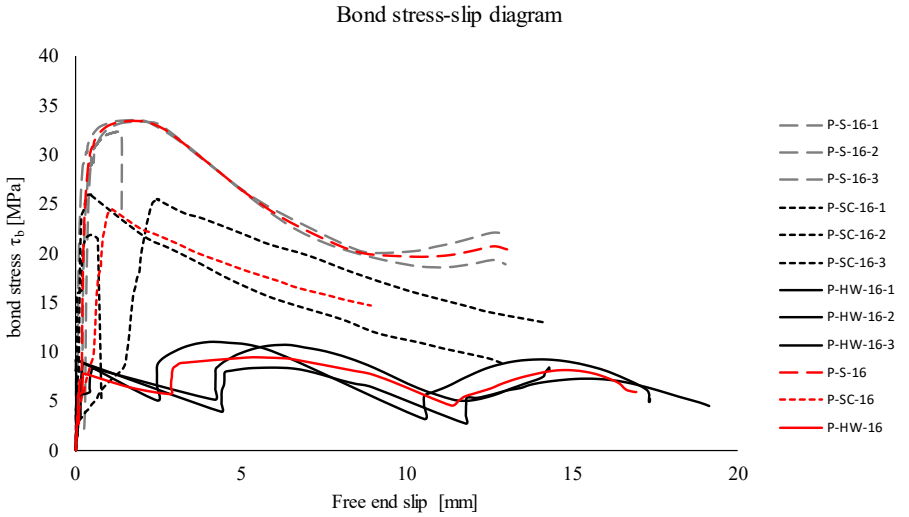

Figure 4.9 Bond stress–slip diagram of the pull-out test at the free end of the bar

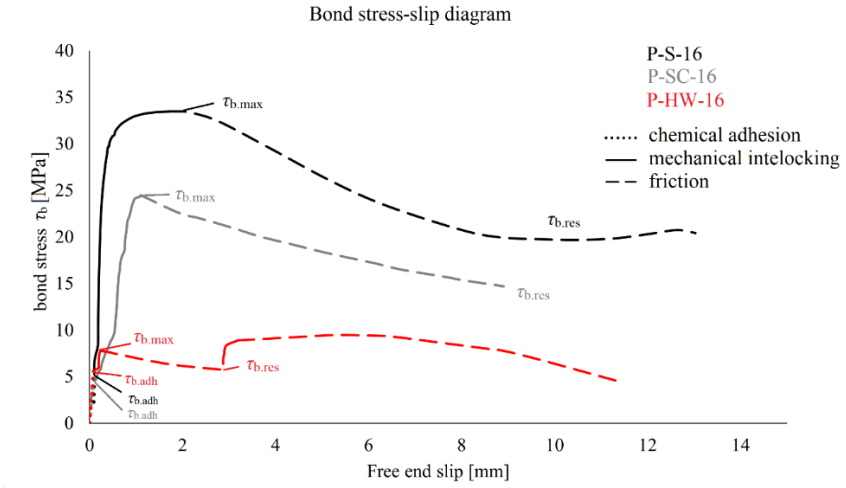

Figure 4.10 Parameters of bond stress–slip diagrams from pull-out tests

4.3. Experimental analysis of bending behaviour of continuous and simple GFRP RC beams

4.3.1. Test specimens

The experimental program consisted of 12 beams: nine continuous beams and three simple beams. All beams had a rectangular cross-section of 200 x 500 mm. The continuous beams had a total length of 5700 mm with two equal effective spans of 2700 mm. The simple beams had a total length of 3000 mm with an identical effective span of 2700 mm as the continuous beams. Two different types of GFRP reinforcement (HW and SC GFRP) and conventional steel were used as longitudinal reinforcement of the beams to evaluate the effect of bond characteristics on the bending behaviour. All beams were reinforced with steel stirrups with a diameter of 8 mm and a spacing of 50 mm through the entire length to prevent shear failure.

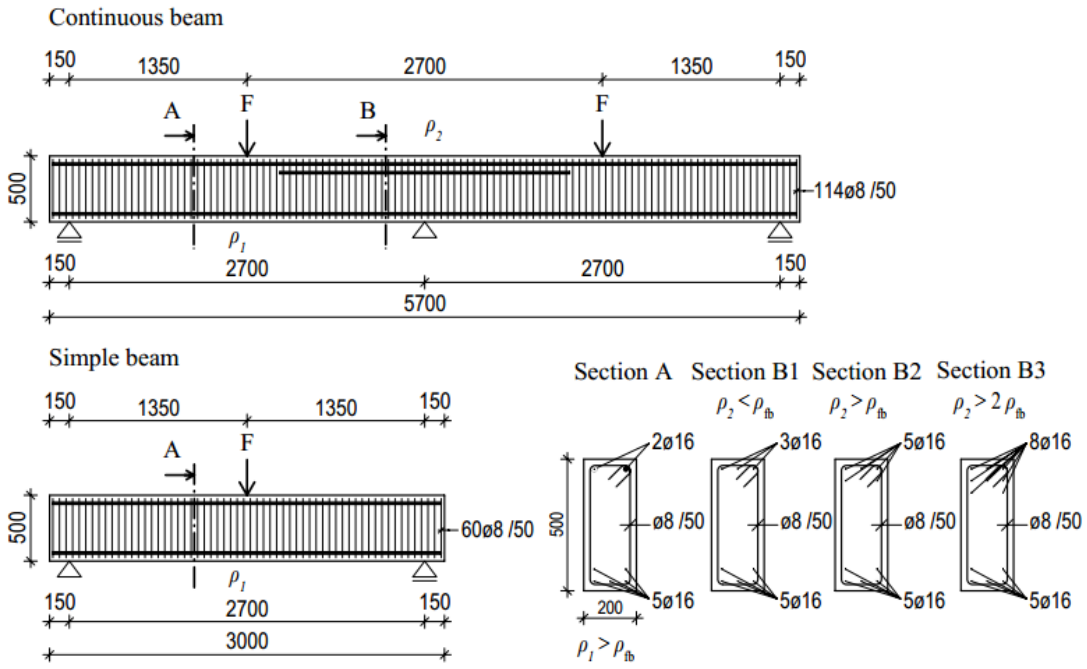

Figure 4.11 Geometry and reinforcement details of tested beams (dimensions in mm)

The area of longitudinal reinforcement at the bottom surface (midspan section) remained constant in all continuous and simple beams. For GFRP-reinforced beams, the aim was to have an over-reinforced midspan section where the reinforcement ratio ρ_1 would be more than ρ_{fb} (ρ_{fb} is the balanced reinforcement ratio of GFRP-reinforced cross-section).

The area of longitudinal reinforcement at the top surface (intermediate support section) distinguished the series of continuous beams. In the case of the GFRP-reinforced continuous beams, the aim for the first series was to have an under-reinforced reinforcement ratio at the intermediate support $\rho_2 < \rho_{fb}$ (see Figure 4.11 section B.1); for the second series, an over-reinforced reinforcement ratio $\rho_2 > \rho_{fb}$ (see Figure 4.11 section B.2); and for the third series significantly over-reinforced reinforcement ratio $\rho_2 > 2\ \rho_{fb}$ (see Figure 4.11 section B.3). The aimed reinforcement ratios of GFRP-reinforced section were reached only in case

of HW GFRP bars. For steel-reinforced continuous beams, the reinforcement area at the bottom and top surface remained the same as for the GFRP-reinforced beams. Table 4.3 shows beam sections' actual reinforcement ratios (ρ) and indicates groups of GFRP-reinforced sections with similar reinforcement ratios for future comparison.

Table 4.3 Reinforcement ratio of beams

Series	Beam notation	Top reinforcement at intermediate support					
		Longitudinal reinforcement	Reinforcement ratio			$A_f E_f$ [kN]	d [mm]
			ρ [%]	ρ_{fb*}[%]	ρ / ρ_{fb}		
1	C-S-A-B1	3Ø16	0.65	-	-	129082	464
	C-SC-A-B1		0.6	1.28	0.47	37544	464
	C-HW-A-B1		0.51	0.67	0.76	25700	465
2	C-S-A-B2	5Ø16	1.14	-	-	215136	441
	C-SC-A-B2		1.06	1.28	0.83	62573	442
	C-HW-A-B2		0.89	0.67	1.33	42834	443
3	C-S-A-B3	8Ø16	1.92	-	-	344218	418
	C-SC-A-B3		1.78	1.28	1.39	100117	419
	C-HW-A-B3		1.5	0.67	2.24	68534	421
Bottom bars at midspan of continuous and simple beams							
0	S-S-A	5Ø16	1.14	-	-	215136	441
	S-SC-A		1.06	1.28	0.83	62573	442
	S-HW-A		0.89	0.67	1.33	42834	443

* The balanced reinforcement ratio for the GFRP-reinforced section (ρ_{fb}) is calculated according to Eurocode 2.

Nomenclature: type of the beam (C - continuous beam, S – simple beam); material of longitudinal reinforcement (S-steel, SC- GFRP with sand-coating, HW- GFRP with helical wrapping); reinforcement configuration at midspan (section A); reinforcement configuration at intermediate support (section B1, B2 or B3)

4.3.2. Test Setup

The test setup for continuous beams consisted of two equal effective spans (2700 mm) supported with two roller supports on the ends and one hinge support in the middle, see Figure 4.12. Concentrated one-point loading was applied at the centre of each span through two hydraulic jacks with a capacity of 1000 kN. Both hydraulic jacks were connected to one hydraulic pump to ensure equal load application at each span. The load-controlled rate was approximately 20 kN/min in 50 kN load steps. Two load cells were used to measure the applied loads, and three were used to measure the reactions at the supports. The deflection was measured with LVDTs and deflection gauges at the middle and in quarters of the spans. LVDT and deflection gauges were placed at the centre of both spans. The rotation of the beam was measured with two spirit levels placed at both ends of the beam. Strain gauges were used to measure the longitudinal reinforcement and concrete

strains at the midspan and intermediate support sections. Muti-frame convergent photogrammetry was performed at each load step. The data from the multi-frame convergent photogrammetry were used to cross-check the deflections, rotation, and strains. Crack propagation was monitored and manually marked at each load step.

The test setup of the simple beams was very similar to that of the continuous beams.

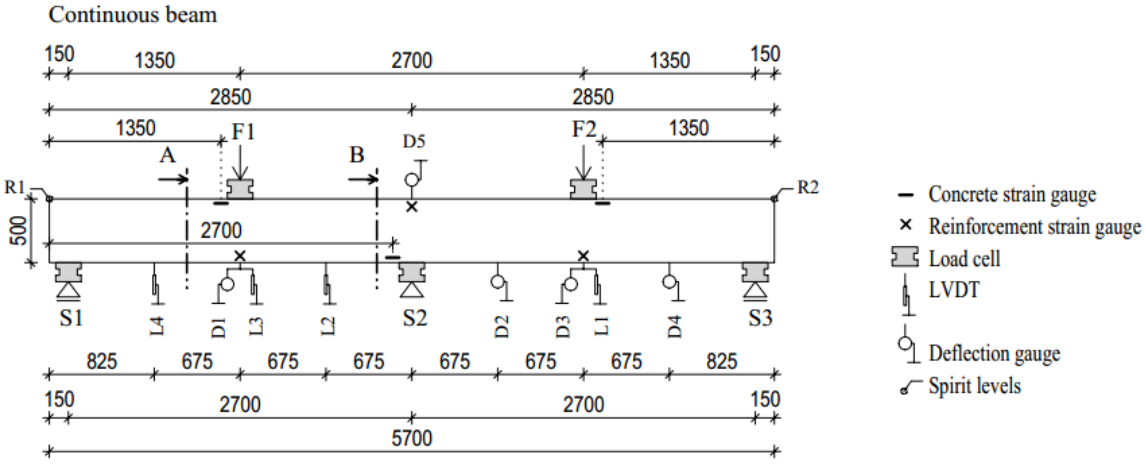

Figure 4.12 Scheme of the test setup of continuous beams (dimensions in mm)

Figure 4.13 Test setup of continuous beams

4.3.3. Test results and discussion

4.3.3.1 Failure modes

Four failure modes were observed during the experimental tests (Conventional ductile flexural failure mode, rupture of the tensile reinforcement, concrete crushing and shear failure). The beams were loaded until the kinematic mechanism was reached, in the case of steel-reinforced beams (formation of two plastic hinges), or until failure occurred in

the case of GFRP-reinforced beams, either by rupture of GFRP bars, concrete crushing, or shear failure. Demonstrated failure modes with reached failure load *F* are summarised in Table 4.4.

Table 4.4 Summary of the observed failure modes

Series	Beam notation	ρ [%]	ρ / ρ_{fb}	Failure load F [kN]	Failure mode
1	C-S-A-B1	0.65	-	455	Yielding at intermediate support followed by midspan
	C-SC-A-B1	0.6	0.47	411	GFRP rupture at intermediate support
	C-HW-A-B1	0.51	0.76	558	GFRP rupture at intermediate support
2	C-S-A-B2	1.14	-	565	Yielding at intermediate support followed by midspan
	C-SC-A-B2	1.06	0.83	548	Shear at intermediate support
	C-HW-A-B2	0.89	1.33	637	Shear at intermediate support
3	C-S-A-B3	1.92	-	599	Yielding at midspan followed by intermediate support
	C-SC-A-B3	1.78	1.39	649	GFRP rupture at midspan
	C-HW-A-B3	1.5	2.24	646	Shear at intermediate support
0	S-S-A	1.14	-	359	Yielding midspan
	S-SC-A	1.06	0.83	401	GFRP rupture at midspan
	S-HW-A	0.89	1.33	404	Concrete crushing

4.3.3.2 Load-bearing capacity

From the beams' failure loads presented in Table 4.4, the load-bearing capacity can be evaluated. The GFRP-reinforced continuous beams within analogous ρ/ρ_{fb} ratios exhibited comparable failure loads. This underscores the reliability of the ρ/ρ_{fb} ratio for comparison in GFRP-reinforced beams rather than the reinforcement ratio ρ alone. Increasing the $\rho/_{\rho fb}$ ratio in the intermediate support section of GFRP-reinforced continuous beams correlated with enhanced load-bearing capacity. Specifically, the transition from a significantly under-reinforced section with a ratio of $0.5\rho_{fb} > \rho/\rho_{fb}$ (yellow) to a slightly under-reinforced section with a ratio of $0.5\rho_{fb} < \rho/\rho_{fb} < \rho_{fb}$ (orange) increased the load-bearing capacity by 35%. Furthermore, the shift from a slightly under-reinforced section (orange) to an over-reinforced section with a ratio of $\rho/\rho_{fb} > \rho_{fb}$ (green) further increased the load-bearing capacity by another 16%. However, further increasing the ρ/ρ_{fb} ratio from an over-reinforced section (green) to a significantly over-reinforced section with $\rho/\rho_{fb} > 2\rho_{fb}$ (blue) did not yield an additional increase in load-bearing capacity. It is crucial to note that the beam with a significantly over-reinforced section (C-HW-A-B3) failed in shear, limiting the load-bearing capacity.

4.3.3.3 Load and moment redistribution

Moment redistribution is quantified by comparing actual and elastic bending moments. The elastic bending moments in critical sections for a given static configuration are 0.156 *Fl* at midspan and 0.188 *Fl* over the intermediate support. Figure 4.14 illustrates that continuous beams reinforced with GFRP exhibited moment redistribution right after cracking. Unlike steel-reinforced members, where redistribution is caused by reaching the designated moment capacity of the intermediate support section, in GFRP-reinforced beams, it arises from variations in critical section stiffness.

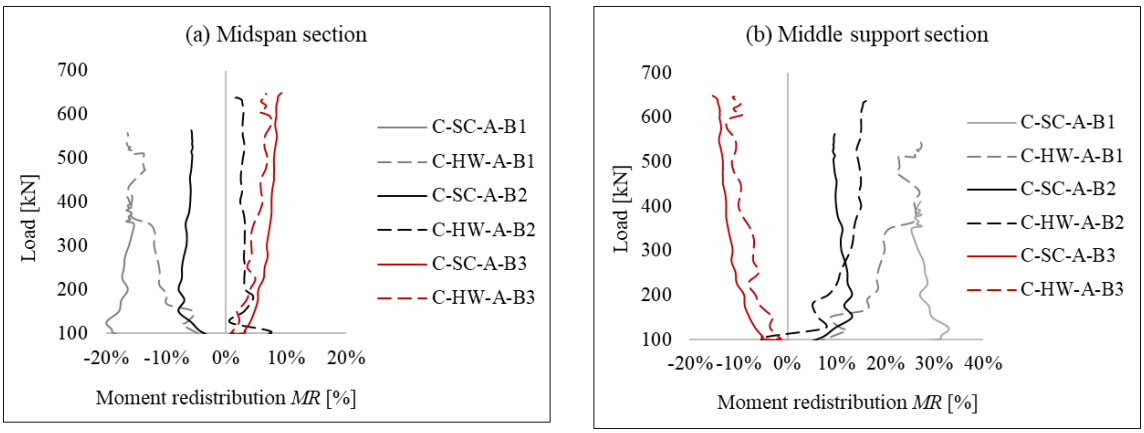

Figure 4.14 Moment redistribution of GFRP-reinforced continuous beams: (a) midspan section, (b) intermediate support section

The GFRP-reinforced beams with an intermediate support section stiffness 67% lower than the midspan (C-SC-A-B1, C-HW-A-B1) effectively redistributed 27% of the hogging moment to the midspan. Conversely, beams with an intermediate support section stiffness 60% higher than the midspan (C-SC-A-B3, C-HW-A-B3) showed an "opposite" redistribution, transferring 7 to 9% of the sagging moment to the intermediate support.

4.3.3.4 Crack patterns and crack width

The flexural cracks started forming at the critical sections of beams during the initial loading stages. Shear cracks in all continuous beams of the second and third series developed around the load step of 450kN (approximately 65-75% of the failure load), propagating between the load points and the intermediate support. During the final loading stage, either the flexural cracks expanded or the shear cracks became predominant and caused the failure.

The surface treatments of GFRP bars had a noticeable impact on crack patterns and crack width development. Beams reinforced with SC GFRP bars formed a higher number of cracks with smaller widths than beams reinforced with HW GFRP bars.

Crack widths in the intermediate support section consistently exhibited faster expansion with increasing moments compared to the midspan section, irrespective of GFRP bar type or ρ/ρ_{fb} reinforcement ratio. Crack widths at the midspan section, where the

reinforcement ratio remained constant, displayed consistent development across all tested GFRP-reinforced beams.

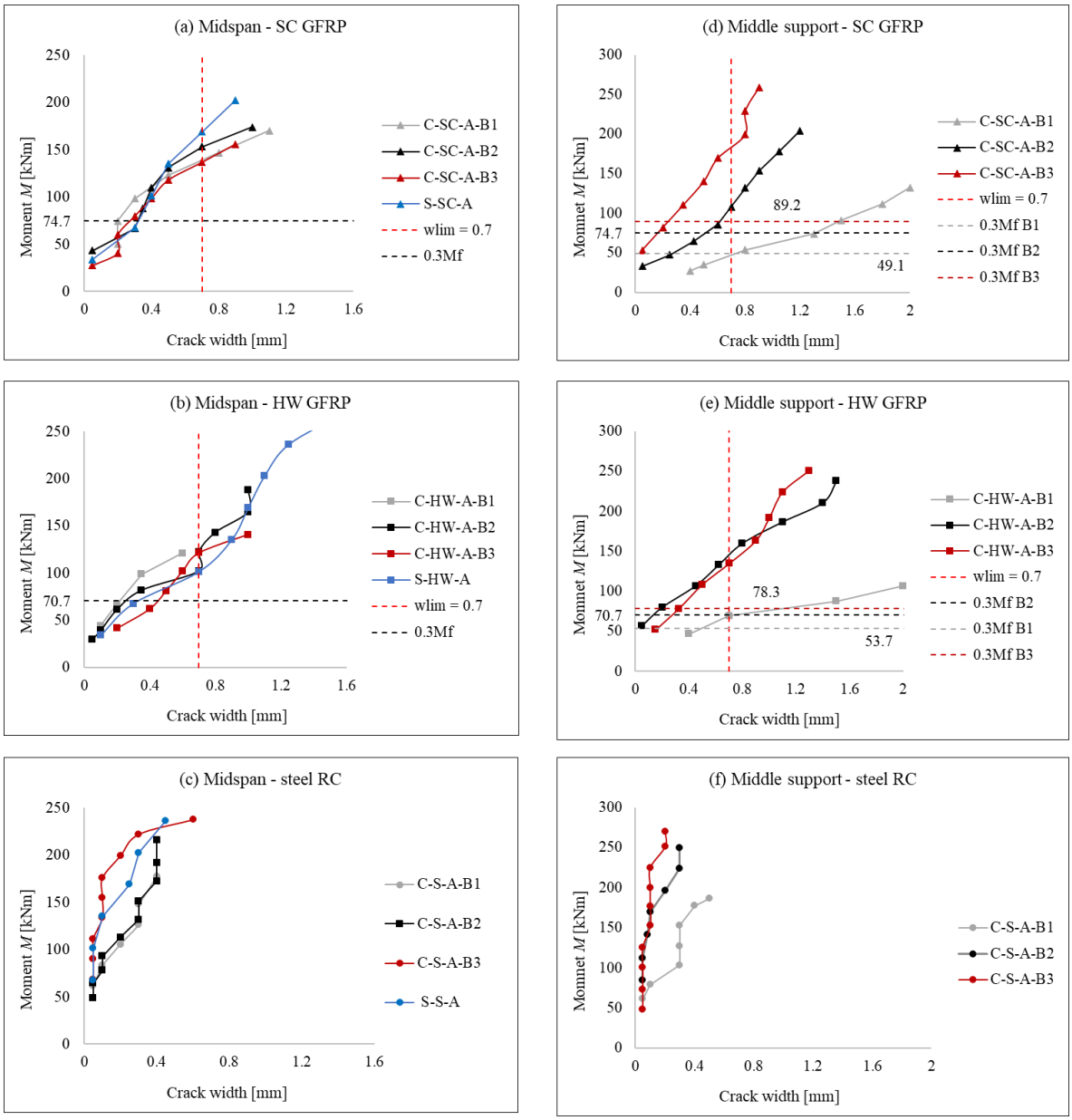

Figure 4.15 Moment-to-crack width relationship: (a) midspan section of SC GFRP-reinforced beams, (b) midspan section of HW GFRP-reinforced beams, (c) midspan section steel-reinforced beams, (d) intermediate support section of SC GFRP-reinforced beams, (e) intermediate support section of HW GFRP-reinforced beams, (f) intermediate support section steel-reinforced beams.

Most GFRP-reinforced beams, except one, met the serviceability criteria at service load. Only the significantly under-reinforced beam C-SC-A-B1, exhibited a crack width of 0.73 mm at a service load of $0.3M_{Rf}$.

4.3.3.5 Load deflection response

The load-deflection curves obtained from LVDT positioned at the middle of the span of all tested beams are presented in Figure 4.16. Beams reinforced with both types of GFRP bars exhibited similar load-deflection responses, suggesting that the surface treatment of GFRP bars has minimal influence on the load-deflection response.

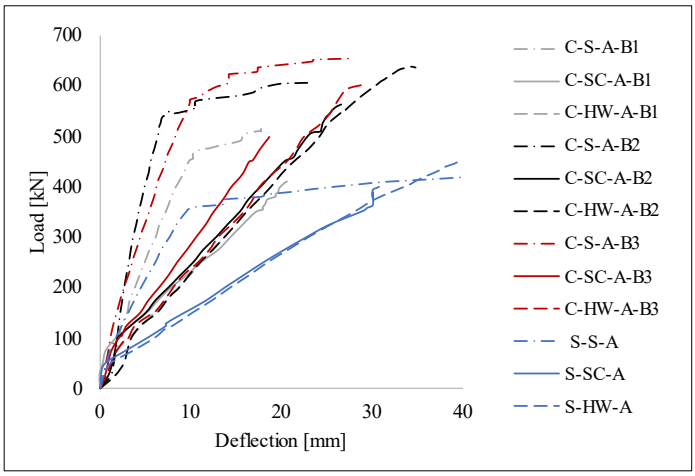

Figure 4.16 Load-deflection response of all tested beams obtained from LVDT

A notable decrease in midspan deflection, ranging from approximately 37% to 52% for SC GFRP RC beams and 40% to 49% for HW GFRP RC beams, was evident when comparing simple and continuous GFRP beams with identical span lengths. Moreover, the reinforcement ratio at the intermediate support section significantly influenced the midspan deflection of GFRP-reinforced continuous beams. The increase of reinforcement ratio from under-reinforced section ($\rho/\rho_{fb} < 0.5$) in the first series to a reinforcement ratio closer to a balanced reinforcement ratio (ρ_{fb}) in the second series resulted in a deflection reduction of approximately 24% and 13% for SC and HW GFRP RC beams, respectively.

The deflection limit values of l/250 were attained at around 40% and 50% of the ultimate load for simple and continuous GFRP-reinforced beams, respectively.

5. Experimental results and code compliance

5.1. Bending capacity and failure load

The experimental and predicted bending capacities for SC and HW GFRP-reinforced beams are compared in Figure 5.1. Under-reinforced sections generally did not reach predicted capacities, highlighting code anticipation of compression-controlled failures. Conversely, over-reinforced sections mostly surpassed predictions. Eurocode, Model Code, and Japanese design codes tend to be more conservative than American and Canadian codes. Specifically, for over-reinforced midspan sections of HW GFRP-reinforced beams, the predicted and experimental values exhibit a 16% discrepancy. Moreover, discrepancies in moment predictions for over-reinforced intermediate support sections range from 22% to 40%.

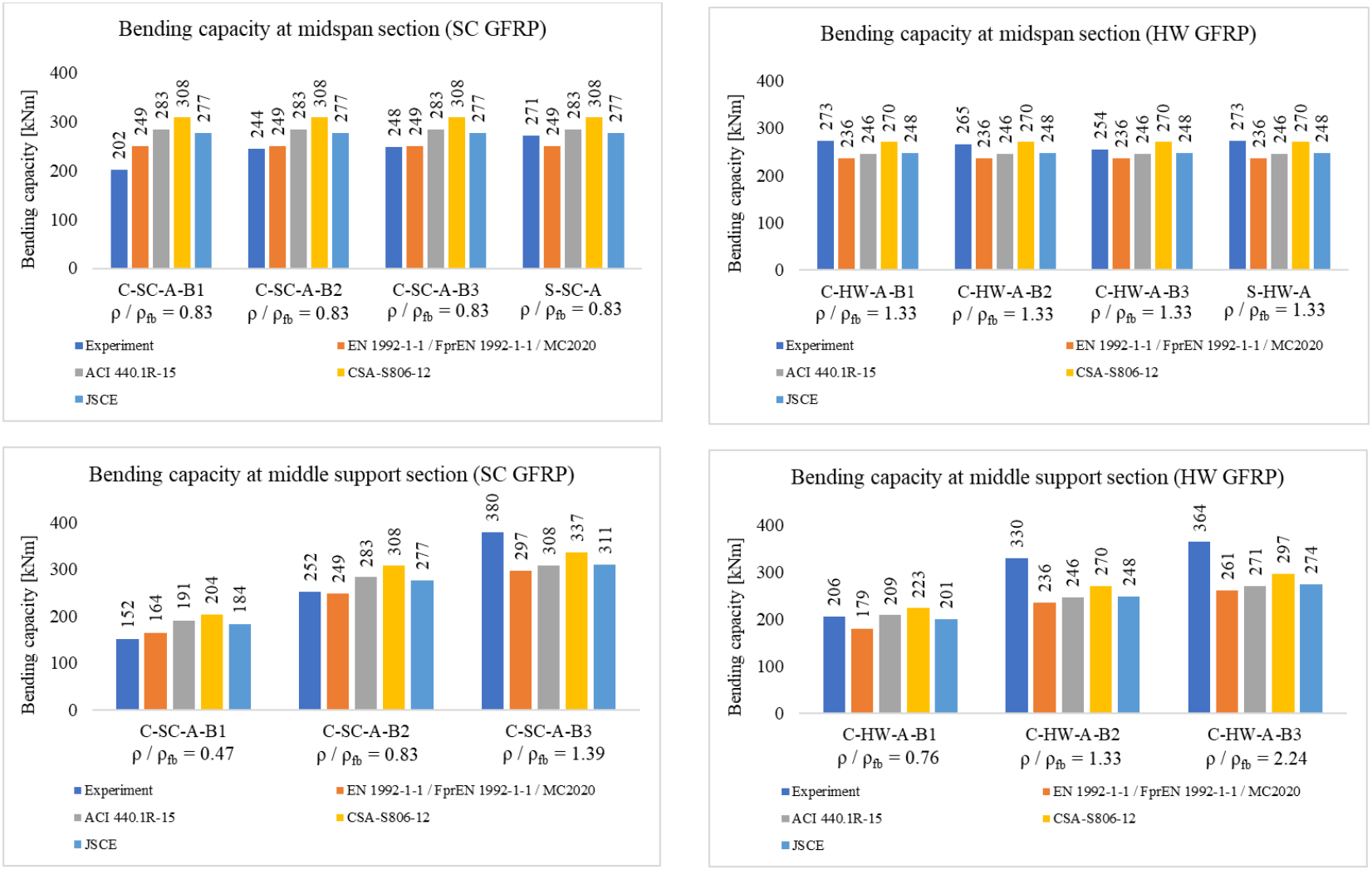

Figure 5.1 Bending capacity of critical sections reinforced with SC GFRP bars (left), bending capacity of critical sections reinforced with HW GFRP bars (right)

5.2. Crack width and bond-dependent coefficient

All the crack width predictions in different parts of their equations incorporate the bond-dependent coefficient (k_b), which accounts for the degree of the bond between the FRP bar and the surrounding concrete. The calculated crack widths according to current Codes of practice using the recommended values of the bond-dependent coefficient (k_b) are compared with measured crack widths in Table 5.1.

Most predictions at the intermediate support section of SC and HW GFRP-reinforced beams underestimated the measured crack widths of under-reinforced and over-reinforced sections, as seen in Table 5.1. These findings underscore the challenge of accurately predicting crack widths at the intermediate support section of continuous GFRP-reinforced beams. On the other hand, crack width predictions at the midspan section of continuous beams aligned well with measured strains at service load. Since the midspan sections of GFRP-reinforced beams made of the same GFRP bar type are identical and the moment-to-crack width relationship is similar The predicted crack widths at the midspan of HW GFRP-reinforced beams using the conservative bond-dependent coefficients recommended by codes and the measured crack widths are in good agreement.On the contrary, the predicted crack widths of SC GFRP-reinforced beams using k_b values recommended by codes mostly overestimated the measured crack widths, indicating the need to reduce the k_b value for SC GFRP bars.

Adjusting the bond-dependent coefficient (k_b) values for the specific types of GFRP reinforcement utilized in this study could enhance the accuracy of crack width predictions outlined in the codes. Canadian design code CSA S806-12 defines in Annex S equation to determine the bond-dependent coefficient (k_b) value from experimental bending tests. According to equation in CSA S806-12, SC GFRP bars exhibit an average k_b value of 0.7, indicating a superior bond to concrete than deformed steel bars, and HW GFRP bars display a calculated average k_b value of 1.36, corresponding to an inferior bond to concrete than steel bars. The calculated crack widths using the adjusted values of the bond-dependent coefficient (k_b) are compared with measured crack widths in Table 5.2.

Adjusting the bond-dependent coefficients (k_b) resulted in ACI, CSA and Eurocode 2 predictions aligning more closely with measured crack widths. For midspan sections of HW GFRP-reinforced beams, the average experimental-to-predicted crack widths (w_{exp} / w_{pred}) ratios were adjusted to 0.84 – 1.0. The higher k_b value for HW GFRP bars also led to more conservative crack width predictions at the intermediate support section. Regarding SC GFRP-reinforced beams, the average experimental-to-predicted crack widths (w_{exp} / w_{pred}) ratios at the midspan section were adjusted to 0.59 – 1.0. However, it is noteworthy that adjusting the k_b value for SC GFRP-reinforced beams resulted in significantly overestimated crack width predictions at the intermediate support section. On the contrary, the MC2020 and FrpEN predictions with adjusted bond-dependent coefficients (k_b) values did not align better with measured crack widths, indicating that these codes need a different approach to determine FRP bars' bond-dependent coefficients (k_b) values.

Table 5.1 Experimental-to-predicted crack widths (w_{exp} / w_{pred}) of GFRP-reinforced beams

Beam	w_{exp} / $w_{pred.ACI}$		w_{exp} / $w_{pred.CSA}$		w_{exp} / $w_{pred.JSCE}$		w_{exp} / $w_{pred.EN}$		w_{exp} / $w_{pred.MC}$		w_{exp} / $w_{pred.FrpEN}$	
	Midspan	Intermediate support	Midspan	Intermediate support	Midspan	Intermediate support	Midspan	Intermediate support	Midspan	Intermediate support	Midspan	Intermediate support
C-SC-A-B1	0.4	1.7	0.6	2.6	0.4	1.8	0.4	2.1	0.3	1.7	0.2	1.1
C-SC-A-B2	0.5	1.7	0.7	2.3	0.5	1.7	0.6	2.1	0.4	2.0	0.4	1.1
C-SC-A-B3	0.4	0.8	0.6	1.0	0.5	0.8	0.5	1.3	0.3	1.0	0.3	0.5
S-SC-A	0.3	-	0.5	-	0.4	-	0.3	-	0.2	-	0.2	-
Average	**0.42**		**0.58**		**0.44**		**0.46**		**0.30**		**0.28**	
C-HW-A-B1	0.9	1.2	1.3	1.7	0.9	1.2	1.0	1.4	0.8	1.1	0.6	0.8
C-HW-A-B2	1.1	0.3	1.5	0.4	1.1	0.3	1.3	0.4	1.2	0.4	0.7	0.2
C-HW-A-B3	0.8	0.9	1.1	1.2	0.8	1.0	1.1	1.5	0.7	1.2	0.5	0.6
S-HW-A	0.5	-	0.7	-	0.5	-	0.5	-	0.4	-	0.3	-
Average	**0.82**		**1.13**		**0.83**		**1.00**		**0.78**		**0.53**	

* k_b = 1.4 was used for ACI 440.1R; k_b = 1.2 was used for CSA S806-12, JSCE, EN 1992-1-1, MC2020, Frp EN 1992-1-1

Table 5.2 Experimental-to-predicted crack widths (w_{exp} / w_{pred}) of GFRP-reinforced beams with adjusted bond-dependent coefficients

Beam	w_{exp} /$w_{pred.ACI}$		w_{exp} /$w_{pred.CSA}$		w_{exp} /$w_{pred.EN}$		w_{exp} /$w_{pred.EN}$		w_{exp} /$w_{pred.EN}$	
	Midspan	Middle support	Midspan	Middle support	Midspan	Middle support	Midspan	Middle support	Midspan	Middle support
C-SC-A-B1	0.8	3.5	1.0	4.4	0.5	2.8	0.2	1.1	0.2	1.1
C-SC-A-B2	1.1	3.3	1.3	3.9	0.8	2.8	0.3	1.4	0.4	1.3
C-SC-A-B3	0.9	1.6	1.0	1.7	0.6	1.6	0.2	0.7	0.4	0.8
S-SC-A	0.7	-	0.8	-	0.4	-	0.1	-	0.3	-
Average	**0.85**		**1.00**		**0.59**		**0.21**		**0.33**	
C-HW-A-B1	0.9	1.2	1.1	1.5	0.9	1.3	0.9	1.2	0.6	0.8
C-HW-A-B2	1.1	0.3	1.4	0.4	1.3	0.4	1.3	0.4	0.7	0.2
C-HW-A-B3	0.8	1.0	0.9	1.1	1.0	1.4	0.8	1.3	0.5	0.6
S-HW-A	0.5	-	0.6	-	0.5	-	0.4	-	0.3	-
Average	**0.84**		**1.00**		**0.93**		**0.85**		**0.53**	

* k_b = 0.7 was used for SC GFRP bars; k_b = 1.36 was used for HW GFRP bars.

6. Conclusion

6.1. Summary

The application of GFRP bars in continuous beams resulted in enhancing the load-bearing capacity and reduction of the span deflection. However, the study also uncovered challenges related to crack expansion at the midspan section, posing difficulties in crack width predictions. In most cases, discrepancies between measured and predicted crack widths (w_{exp} / w_{pred}) indicated an underestimation of crack width at the intermediate support section. Furthermore, examining surface treatment effects on bending behaviour revealed significant influences on crack formation and width, emphasizing the importance of experimentally determining bond-dependent coefficient (k_b) values. Despite variations in surface treatment, bending capacity and deflection were not notably affected; instead, tensile properties such as tensile strength (f_{fu}) and modulus of elasticity (E_f) played dominant roles.

6.2. Conclusions

The following conclusions may be stated:

1. Experimental determination of bond:
   a) The consistency in bond stress development between both testing methods (beam bond test, pull-out test) reaffirms the reliability of the employed approaches. However, a significant variation is evident in the bond stress-slip diagrams of GFRP bars. These bars exhibited increased sensitivity to loading differences in the bond tests. In beam bond tests, loading ceases upon the initial failure at the surface of the GFRP bar. In contrast, the pull-out test involves continued loading, enabling the observation of residual friction of the GFRP bar. Moreover, the pull-out tests give more conservative values of bond strength ($\tau_{b.max}$) of GFRP bars.
   b) Generally, the results of locally available GFRP bars showed lower bond strength ($\tau_{b.max}$) than steel bars. In beam tests, the SC GFRP bars reached 78%, and HW GFRP bars only 36% of the steel bars' average bond strength ($\tau_{b.max}$). In pull-out tests, the ratio is 76% and 27% of the steel bars' average bond strength ($\tau_{b.max}$) by SC GFRP and HW GFRP bars, respectively.
   c) The sand-coated surface, as opposed to the helically wrapped surface, increased bond strength by 54% in beam tests and 64% in pull-out tests, demonstrating its effectiveness in enhancing the bond to concrete.
2. Experimental analysis of bending behaviour of GFRP RC beams:
   a) The GFRP-reinforced continuous beams within analogous ρ/ρ_{fb} ratios exhibited comparable failure loads. The increase of ρ/ρ_{fb} ratio in the intermediate support section of GFRP-reinforced continuous beams correlated with enhanced load-bearing capacity.
   b) The continuous beams reinforced with GFRP displayed immediate moment redistribution upon cracking arising from variations in critical section stiffness. Beams with an intermediate support section stiffness 67% lower than the midspan (C-SC-A-B1, C-HW-A-B1) effectively redistributed 27% of the hogging moment to

the midspan. Conversely, beams with an intermediate support section stiffness 60% higher than the midspan (C-SC-A-B3, C-HW-A-B3) showed an "opposite" redistribution, transferring 7 to 9% of the sagging moment to the intermediate support.

c) The surface treatments of GFRP bars had a noticeable impact on crack patterns and crack width development. Beams reinforced with SC GFRP bars formed a higher number of cracks with smaller widths than beams reinforced with HW GFRP bars. The bond-dependent coefficient (k_b) analysis based solely on surface configuration further supported this, revealing smaller k_b values for SC GFRP bars (0.7) than HW GFRP bars (1.36).
d) Crack widths in the intermediate support section consistently exhibited faster expansion with increasing moments compared to the midspan section, irrespective of GFRP bar type or ρ/ρ_{fb} reinforcement ratio. Code predictions underestimated the crack width at the intermediate support section.
e) Crack widths in the intermediate support section exhibited a notable decrease with increasing reinforcement ratio, particularly in SC GFRP-reinforced beams. Over-reinforcing the intermediate support section of continuous GFRP-reinforced beams can effectively limit crack widths to meet serviceability requirements.
f) Crack widths at the midspan section, where the reinforcement ratio remained constant, displayed consistent development across all tested GFRP-reinforced beams. Design codes reasonably predicted crack widths for HW GFRP-reinforced beams using recommended bond-dependent coefficients (k_b) values. Nevertheless, adjusting the k_b values following the equation defined in CSA S806-12 Annex S led to code predictions (w_{pred}) aligning more closely with measured crack widths (w_{exp}).
g) Surface treatment does not affect beam deflection. The reinforcement ratio at the intermediate support section significantly influenced the midspan deflection of GFRP-reinforced continuous beams.
h) The deflection limit values of $l/250$ were attained at around 40% and 50% of the ultimate load for simple and continuous GFRP-reinforced beams, respectively. A notable decrease in midspan deflection, ranging from approximately 37% to 52% for SC GFRP RC beams and 40% to 49% for HW GFRP RC beams, was evident when comparing simple and continuous GFRP beams with identical span lengths.
i) Experimental bending moments (M_{exp}) of under-reinforced sections ($\rho/\rho_{fb} < 1$) generally fell short of predicted capacities (M_{cal}), highlighting that the FRP design codes typically anticipate compression-controlled failure. Conversely, over-reinforced sections ($\rho/\rho_{fb} > 1$) mostly exceeded predicted bending moments.

6.3. Contribution for engineering practice

- This study underscores the significance of experimental determination of tensile properties, particularly tensile strength (f_{fu}) and modulus of elasticity (E_f) of GFRP bars, as these values vary among manufacturers. Furthermore, the nonhomogenous nature of GFRP bars may result in disparities between the experimentally tested and stated values from manufacturers.

- The design of GFRP-reinforced members is governed by the serviceability limit state criteria (cracking and deflection) that are reached at 30-50% of the bending capacity.
- The bending capacity of over-reinforced sections ($\rho/\rho_{fb} > 1$) in continuous GFRP-reinforced members tends to surpass the predicted bending capacity by up to 40%. Conversely, the design codes can accurately predict the bending capacity of simple GFRP-reinforced beams.
- GFRP-reinforced continuous beams with under-reinforced intermediate support sections ($\rho/\rho_{fb} < 1$) exhibit rapid crack expansion at the intermediate support section, which deviates from crack width predictions (w_{pred}).
- The design of over-reinforced GFRP sections in continuous beams can lead to meeting the serviceability limit state criteria (cracking and deflection) and further possibilities in structural application.
- Adjusting the bond-dependent coefficient (k_b) values for the specific types of GFRP reinforcement is crucial to enhance the accuracy of crack width predictions outlined in the codes.

6.4. Proposal for the future work

- Investigation of continuous GFRP-reinforced beams with an over-reinforced middle-support section focused on the serviceability limit state criteria.
- Investigation of the influence of bond-dependent coefficient (k_b) values on the precision of crack width predictions in simple and continuous beams reinforced with FRP bars with different fibre types, diameters, surface treatments, and varying concrete strengths.

7. References

[1] RILEM, *I. Recommendations for reinforcing steels - Recommendations applicable both to reinforcing steels and to prestressing steels*, vol. 6, no. 5. 1973. doi: 10.1007/BF02473623.

[2] ACI Committee 440, *Guide test methods for fiber-reinforced polymers (FRP) composites for reinforcing or strengthening concrete and masonry structures*. 2012.

[3] "KOMPOZITNÍ VÝZTUŽE PREFA Rebar PREFA Carb." [Online]. Available: www.prefa-kompozity.cz

[4] "https://fiberox.eu/."

[5] I. Standard, *ISO 6892-1 Metallic materials — Tensile testing — Part 1: Method of test at room temperature 1*. 2009.

[6] E. Gudonis, R. Kacianauskas, V. Gribniak, A. Weber, R. Jakubovskis, and G. Kaklauskas, "Mechanical Properties of the Bond Between GFRP Reinforcing Bars and Concrete," *Mechanics of Composite Materials*, vol. 50, no. 4, pp. 457–466, 2014, doi: 10.1007/s11029-014-9432-0.

[7] M. Štefanovičová, K. Gajdošová, R. Sonnenschein, and V. Borzovič, "Experimental evaluation of the bond Between concrete and GFRP bars with different surface treatments," *J Compos Mater*, vol. 56, no. 22, 2022, doi: 10.1177/00219983221114695.

[8] O. Janus, F. Girgle, L. Bodnarova, and V. Kostiha, "The effect of various test configurations on the bond strength of sand-coated GFRP bars The Effect of Various Test Configurations on the Bond Strength of Sand-Coated GFRP Bars," vol. 020002, no. February, 2020.

[9] L. Chiriatti, H. Mercado-Mendoza, K. L. Apedo, C. Fond, and F. Feugeas, "A study of bond between steel rebar and concrete under a friction-based approach," *Cem Concr Res*, vol. 120, pp. 132–141, Jun. 2019, doi: 10.1016/j.cemconres.2019.03.019.